Journal of Solid State Chemistry 182 (2009) 1638–1648

Contents lists available at ScienceDirect

Journal of Solid State Chemistry

journal homepage: www.elsevier.com/locate/jssc

Structural and magnetic properties of $Pr_{18}Li_8Fe_{5-x}M_xO_{39}$ (M = Ru, Mn, Co)

Siân E. Dutton [a], Peter D. Battle [a,*], Fernande Grandjean [b], Gary J. Long [c,*], Moulay T. Sougrati [b], Peter A. van Daesdonk [a], Emma Winstone [a]

[a] Inorganic Chemistry Laboratory, Department of Chemistry, University of Oxford, South Parks Road, Oxford OX1 3QR, UK
[b] Department of Physics, University of Liège, B5, B-4000 Sart-Tilman, Belgium
[c] Department of Chemistry, Missouri University of Science and Technology, University of Missouri-Rolla, Rolla, MO 65409-0010, USA

ARTICLE INFO

Article history:
Received 16 February 2009
Received in revised form
30 March 2009
Accepted 2 April 2009
Available online 9 April 2009

Keywords:
Mixed-metal oxide
Magnetism
Neutron diffraction
Mössbauer spectroscopy

ABSTRACT

A polycrystalline sample of $Pr_{18}Li_8Fe_4RuO_{39}$ has been synthesized by a solid state method and characterized by neutron powder diffraction, magnetometry and Mössbauer spectroscopy; samples of $Pr_{18}Li_8Fe_{5-x}Mn_xO_{39}$ and $Pr_{18}Li_8Fe_{5-x}Co_xO_{39}$ ($x = 1, 2$) have been studied by magnetometry. All these compounds adopt a cubic structure (space group $Pm\bar{3}n$, a_0~11.97 Å) based on intersecting ⟨111⟩ chains made up of alternating octahedral and trigonal-prismatic coordination sites. These chains occupy channels within a Pr–O framework. The trigonal-prismatic site in $Pr_{18}Li_8Fe_4RuO_{39}$ is occupied by Li^+ and high-spin Fe^{3+}. The remaining transition-metal cations occupy the two crystallographically-distinct octahedral sites in a disordered manner. All five compositions adopt a spin-glass-like state at 7 K ($Pr_{18}Li_8Fe_4RuO_{39}$) or below.

1. Introduction

The crystal structure of $Ln_{18}Li_8Rh_5O_{39}$ (Ln = La, Pr) has been reported previously [1]. Chains of coordination polyhedra, in which octahedral sites alternate with trigonal-prismatic sites, occupy channels within a Ln–O framework, as shown in Fig. 1. The chains run along the ⟨111⟩ directions of the cubic unit cell (space group $Pm\bar{3}n$) and intersect each other at (0, 0, 0) and $(\frac{1}{2}, \frac{1}{2}, \frac{1}{2})$. Equivalent octahedral sites are located at these two points of intersection and a further, crystallographically-distinct octahedral site is located halfway between them; the two distinct types of octahedral site are always separated from each other by a prismatic site which is occupied by Li^+. The rhodium cations, which occur as Rh^{3+} and Rh^{4+} in a ratio of 4:1, are distributed over two distinct octahedral sites which have multiplicities of 8 and 2 within the unit cell. The Rh^{3+} and Rh^{4+} cations occupy the 8-fold and 2-fold sites, respectively; the former site is significantly larger than the latter and the size difference drives the cation ordering.

The presence of two crystallographically-distinct sites provides an opportunity to order cations of different elements, rather than simply different oxidation states of the same element. If these cations have different magnetic moments then it might be possible to produce ferrimagnetic materials that have a spontaneous magnetization below some critical temperature, even if the dominant superexchange interaction is antiferromagnetic in nature; there is an analogy here with spinel oxides, although in that case the two sites have different coordination numbers as well as different sizes. We envisage antiferromagnetic coupling between the octahedrally-coordinated transition-metal cations along each body-diagonal of the unit cell; this coupling can propagate through the structure, in this case through the trigonal-prismatic site, without frustration.

In an attempt to make new ferrimagnets we originally prepared [2,3] a number of compositions having the general formula $Nd_{18}Li_8M_4M'O_{39}$, where M and M' are 3d elements. Unfortunately M and M' did not order over the two crystallographic sites and, in some cases, site exchange occurred between Li^+ and M. Consequently these compositions show spin-glass-like magnetic behaviour rather than ferrimagnetism. Although the electronic properties of mixed-metal oxides containing open-shell transition-metal cations are largely determined by the d-electron configuration of that cation, the influence of any lanthanide or alkaline-earth cations present cannot be neglected. These cations play a decisive rôle in determining the details of the structural chemistry of the compound, and small changes in crystal structure can produce large changes in the electronic properties. In some cases a particular crystal structure or cation-ordering pattern might only be stable in the presence of the one lanthanide cation that has the appropriate ionic radius [4]. In this paper we describe our attempts to synthesize compounds having two different d-block elements distributed over the two octahedral sites of this crystal structure, with the cation sites in the Ln–O framework being occupied by Pr^{3+} rather than Nd^{3+}.

* Corresponding authors. Fax: +44 1865 272690 (P.D. Battle).
E-mail addresses: Peter.Battle@chem.ox.ac.uk (P.D. Battle), glong@mst.edu (G.J. Long).

0022-4596/$ - see front matter © 2009 Elsevier Inc. All rights reserved.
doi:10.1016/j.jssc.2009.04.002

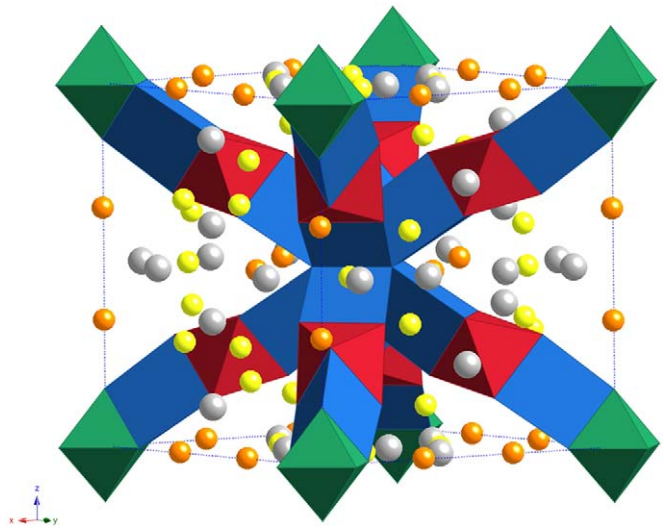

Fig. 1. The cubic $Ln_{18}Li_8Rh_5O_{39}$ structure (space group $Pm\bar{3}n$); grey circles represent oxygen (O2 and O3), yellow circles Ln1, and orange circles Ln2. The LiO_6 trigonal prisms are blue (16*i* site), the RhO_6 octahedra are green (2*a* site) and red (8*e* site). An additional 2*a* site is located at the centre of the unit cell.

Considerations of ionic size and redox chemistry resulted in ruthenium, iron, manganese and cobalt being chosen as the *d*-block elements. Our general aim was to investigate how wide a range of compositions this structure could accommodate, and, in particular, whether the increase in radius of the framework cation would result in ferrimagnetism. The choice of lanthanide cation proved to be particularly important in the case of the iron–ruthenium system, and consequently $Pr_{18}Li_8Fe_4RuO_{39}$ became the focus of our study.

2. Experimental

Attempts were made to synthesise pure samples of $Pr_{18}Li_8Fe_{5-x}M'_xO_{39}$ (M' = Ru, Mn, Co; $0 \leqslant x \leqslant 5$). Stoichiometric quantities of oxide starting materials (praseodymium(III, IV) oxide (99.996%, Alfa Aesar), manganese(IV) oxide (99.999%, Alfa Aesar), iron(III) oxide (99.998%, Alfa Aesar), cobalt(II, III) oxide (99.9985%, Alfa Aesar), ruthenium(IV) oxide (99.95, Alfa Aesar)) were ground together along with a 50% excess of the highly volatile lithium carbonate (AnalaR) prior to firing in pellet form at 800 °C in air overnight. A further 50% excess lithium carbonate was ground into the reaction mixture before it was fired again in air for one hour, as a pellet, at 1000 °C. X-ray powder diffraction was used to monitor the progress of the reactions. Further one-hour firings, with the addition of 50% excess lithium carbonate, were carried out on samples that X-ray powder diffraction showed to be impure at this stage.

All X-ray powder diffraction was carried out on a Philips X'pert diffractometer operating with Cu$K\alpha_1$ radiation with a step size of $\Delta 2\theta = 0.0084°$. X-ray powder diffraction data with a high signal to noise ratio were collected over a small angular range ($15 \leqslant 2\theta/° \leqslant 40$) in order to detect lithium-containing impurities. High-resolution X-ray powder diffraction data for use in quantative analysis were collected over the angular range $5 \leqslant 2\theta/° \leqslant 125$. Rietveld [5] refinement of the structures were carried out using the GSAS [6] suite of programs. Backgrounds were fitted using a Chebyshev polynomial of the first kind and the peak shape was modelled using a pseudo-Voigt function.

Neutron powder diffraction data were collected on $Pr_{18}Li_8Fe_4RuO_{39}$ using the diffractometer *D2b* at the Institut Laue Langevin, Grenoble, France. *D2b* is a high-flux, high-resolution instrument that operates at a wavelength $\lambda = 1.59147$ Å. Data were collected over the angular range $5 \leqslant 2\theta/° \leqslant 160$ with a step size $\Delta 2\theta = 0.05°$ at room temperature. The sample (0.59 g) was contained within a vanadium can ($\phi = 5$ mm). Rietveld refinement of the structure was carried out using the FULLPROF [7] program. The background was estimated manually and then refined using the software. Peak shapes were modelled using a pseudo-Voigt function employing three peak-asymmetry parameters in the angular region $2\theta \leqslant 54°$.

Magnetic measurements were carried out using a Quantum Design MPMS 5000 SQUID magnetometer. The magnetization (M) was measured as a function of temperature on warming from 2 to 300 K after cooling both in zero field and in the measuring field of 100 Oe. The isothermal magnetisation was measured as a function of field ($-50 \leqslant H/kOe \leqslant 50$) after cooling to the measuring temperature in 50 kOe. AC susceptibility data were recorded at up to 11 frequencies ($0.5 \leqslant \omega/Hz \leqslant 1000$) in a direct field of ~2 Oe and an oscillating field of amplitude 3.5 Oe over an appropriate temperature range with $\Delta T = 0.1$ K.

The Mössbauer spectra of $Pr_{18}Li_8Fe_4RuO_{39}$ have been measured between 4.2 and 295 K in a Janis Supervaritemp cryostat with a constant-acceleration spectrometer which utilized a rhodium matrix cobalt-57 source and was calibrated at room temperature with α-iron powder. The Mössbauer spectral absorber contained 33 mg/cm^2 of powder mixed with boron nitride. The ideal thickness of the Mössbauer absorber is limited to this value because of the strong non-resonant scattering of the γ-rays by the 18 praseodymium ions. This effect is, at least in part, responsible for the rather low signal to noise ratio observed at 4.2 and 7 K. For the 8*e* site the relative statistical errors associated with the isomer shifts, quadrupole splittings, and line widths are ± 0.005, ± 0.01, and ± 0.01 mm/s, respectively; these errors are approximately twice as large for the 2*a* and 16*i* sites. The absolute errors of these parameters are twice the statistical errors.

3. Results

(i) $Pr_{18}Li_8Fe_5O_{39}$: We were unable to prepare a monophasic sample of $Pr_{18}Li_8Fe_5O_{39}$, despite repeated attempts at different heating temperatures.

(ii) $Pr_{18}Li_8Fe_4RuO_{39}$: $Pr_{18}Li_8Fe_4RuO_{39}$ was the only composition in the series $Pr_{18}Li_8Fe_{5-x}Ru_xO_{39}$ ($1 \leqslant x \leqslant 5$) to be synthesized successfully. In this case, X-ray diffraction data indicated the formation of a monophasic product isostructural with $La_{18}Li_8Rh_5O_{39}$ and having a unit-cell parameter $a = 12.0318(2)$ Å. The dominance of the scattering by the heavy ions rendered impossible a full structural refinement based on the X-ray data. In addition to the main phase, neutron diffraction data collected on $Pr_{18}Li_8Fe_4RuO_{39}$ revealed the presence of two impurity phases: Li_2CO_3 (2.6(3) wt%) and a spinel [8], Fe_5LiO_8 (0.28(2) wt%); the significance of this is discussed below. The data were analysed in the space group $Pm\bar{3}n$ with the iron and ruthenium cations occupying the 8*e* and 2*a* sites in a disordered manner. There are two distinct Pr^{3+} sites in the asymmetric unit; the oxide ions O2 and O3 are coordinated exclusively to these cations and together they form the Pr–O framework referred to above; no difficulties were encountered in refining the parameters associated with these ions. The oxide ion O1 forms the octahedron around the 8*e* octahedral site and O4 forms the octahedron around the 2*a* octahedral site; O1 and O4 thus form the opposing triangular faces of the 16*i* trigonal-prismatic site. In the idealized structure, O4 would occupy the 12*f* (x, 0, 0) site, but in $La_{18}Li_8Rh_5O_{39}$ it is displaced onto the 48*l* (x, y, z) site with 25% occupancy; it was also necessary to introduce this disorder into the present data analysis. O1 and O4 make additional short contacts to the lanthanide cation and thus provide the link between the *Ln*–O framework and the

polyhedral chains. Preliminary refinements gave a reasonable fit to the data but the displacement parameters associated with the 8*e* and 16*i* sites were found to be large. Structural models in which iron was allowed to occupy the trigonal-prismatic site were therefore considered. Both a lithium-deficient model with vacancies on the 8*e* sites and a model in which the stoichiometry was maintained by allowing lithium to replace iron on some of the 8*e* sites were investigated. It was found that the best model was that in which the $Pr_{18}Li_8Fe_4RuO_{39}$ stoichiometry was maintained, with iron and lithium disordered over the octahedral 8*e* and trigonal-prismatic 16*i* sites. As a consequence of iron partially occupying the trigonal-prismatic site the average scattering power of that site was reduced to approximately zero. It was therefore necessary to constrain the displacement parameter to be zero. Details of the final structural model are given in Tables 1 and 2; the observed and calculated diffraction profiles are shown in Fig. 2.

The zero-field-cooled (ZFC) and field-cooled (FC) magnetic susceptibilities of $Pr_{18}Li_8Fe_4RuO_{39}$ (see Table 3 and Fig. 3) both show a maximum at $T_f = 7.0(3)$ K. On cooling below T_f the ZFC susceptibility decreases steadily whereas the FC susceptibility reaches a minimum at ~3.5 K. Above T_f the inverse susceptibility is linear and fitting the data collected above 100 K to the Curie–Weiss law gives $C = 42.00(8)\,cm^3\,K\,mol^{-1}$ and $\theta = -30.3$ K. The field dependence of the magnetisation at 2 K (Fig. 4) is non-linear, unsaturated at 50 kOe and shows significant hysteresis in fields below $H = 5$ kOe.

The real component of the ac susceptibility, χ', of $Pr_{18}Li_8Fe_4RuO_{39}$ shows (Fig. 5) a frequency dependence at low temperatures: $T_f(1.0\,Hz) = 7.7(1)$ K, $T_f(1000\,Hz) = 8.1$ K, resulting in a value for the parameter $\kappa = \Delta T_f/T_f\Delta \log \omega$ of 0.016. At low frequencies, two distinct features are observed in the imaginary component, χ'', but these are not resolved at the higher measuring frequencies.

Table 1
Structural parameters of $Pr_{18}Li_8Fe_4RuO_{39}$ at room temperature derived from neutron diffraction data.

a/Å		12.03029(3)
R_p		0.059
χ^2		2.02
Pr1 24*k*	*y*	0.3086(6)
0 *y z*	*z*	0.3056(6)
	B_{iso}/Å^2	1.02(9)
Pr2 12*f*	*x*	0.3463(6)
x 0 0	B_{iso}/Å^2	0.40(12)
Fe1(Ru) 2*a*	B_{iso}/Å^2	1.4(3)
0 0 0	Fe occupancy	0.62(10)
	Ru occupancy	0.38(10)
Fe2(Ru/Li) 8*e*	B_{iso}/Å^2	1.5(1)
$\frac{1}{4}\frac{1}{4}\frac{1}{4}$	Fe occupancy	0.69(3)
	Ru occupancy	0.16(3)
	Li occupancy	0.15(3)
Li1(Fe) 16*i*	*x*	0.3681(12)
x x x	B_{iso}/Å^2	0.0
	Fe occupancy	0.076(5)
	Li occupancy	0.924(5)
O1 48*l*	*x*	0.8662(3)
x y z	*y*	0.8597(3)
	z	0.6928(2)
	B_{iso}/Å^2	0.75(4)
O2 6*d*	B_{iso}/Å^2	0.66(13)
$\frac{1}{4}\frac{1}{2}$ 0		
O3 12*g*	*x*	0.6302(6)
x 0 $\frac{1}{2}$	B_{iso}/Å^2	1.24(13)
O4 48*l*	*x*	0.1559(6)
x y z	*y*	0.012(2)
	z	−0.019(1)
	B_{iso}/Å^2	1.3(3)
	Occupancy	0.25

Table 2
Selected bond lengths (Å) and angles (deg) in $Pr_{18}Li_8Fe_4RuO_{39}$ at room temperature.

Pr1–O1	2.587(7) × 2
	2.668(6) × 2
	2.508(4) × 2
Pr1–O2	2.443(7)
Pr1–O3	2.429(7)
	3.123(7)
Pr2–O1	2.379(3) × 4
Pr2–O3	2.423(8) × 2
Pr2–O4	2.307(10)
Fe1(Ru)–O4	1.90(1) × 6
Fe2(Ru/Li)–O1	2.042(3) × 6
Li1(Fe)–O1	2.111(15) × 3
Li1(Fe)–O4	2.27(2)[a] × 3
Li1(Fe)–Li1(Fe)	3.17(2)
Fe1(Ru)–Li1(Fe)	2.748(14)
Fe2(Ru/Li)–Li1(Fe)	2.461(14)
Pr1–Pr1 (pore size)	6.321(3)
O1–Fe2(Ru/Li)–O1	90.4(2)
	87.5(2)
	97.9(2)

[a] Denotes an average of bonds as the oxygen position is disordered.

The iron-57 Mössbauer spectra of $Pr_{18}Li_8Fe_4RuO_{39}$ have been measured between 4.2 and 295 K, see Figs. 6 and 7. The spectra indicate that $Pr_{18}Li_8Fe_4RuO_{39}$ is paramagnetic between 295 and 40 K, just begins to exhibit very weak magnetic broadening at 25 K, exhibits a weak magnetic sextet at 12 K, and exhibits well-resolved magnetic sextets at 7 and 4.2 K.

The paramagnetic spectra obtained at and above 40 K have been fit with three doublets assigned to the 2*a*, 8*e*, and 16*i* sites, respectively; the relative areas of these sites have been constrained to 15.55%, 69.21%, and 15.24%, respectively, the iron occupancy of these crystallographic sites as determined at room temperature by powder neutron diffraction, see Table 1. The resulting fits, see Fig. 6, and the corresponding spectral parameters, see Table 4 and Figs. 8 and 9, although not unique, are most consistent with the electronic properties of $Pr_{18}Li_8Fe_4RuO_{39}$ which formally contains iron(III) ions on the 8*e* and 16*i* crystallographic sites and iron(IV) ions on the 2*a* site. The constraint based on the relative areas of the three components has been applied because the lack of details in the paramagnetic Mössbauer spectra renders several fitting models perfectly satisfactory from the statistical and physical points of view and because a reasonable analysis of the Mössbauer spectra must include all available information and specifically the neutron diffraction results.

The 25 K Mössbauer spectrum of $Pr_{18}Li_8Fe_4RuO_{39}$ is broadened relative to that observed at 40 K as a result of the onset of magnetic interactions. It was found that the best way to account for this broadening was to divide the 8*e* site into a paramagnetic component and a magnetic component with a small field of 0.4 T, see the two red components in the 25 K spectrum shown in Fig. 6; the relative areas for the three sites have been constrained to be the same as at the higher temperatures.

Apparently as a result of small structural changes or perhaps magnetostriction, upon cooling the quadrupole interaction, ΔE_Q, for the 2*a* site increases below ca. 40 K whereas that of the 8*e* and 16*i* sites decreases slightly. All attempts to avoid these changes led to substantially poorer fits.

The 7 and 4.2 K spectra of $Pr_{18}Li_8Fe_4RuO_{39}$ have been fit with the superposition of three sextets, assigned to the 2*a*, 8*e*, and 16*i* sites, respectively, with hyperfine fields of 22(2), 49.3(2), and 43(1) T at 7 K and 44(1), 50.7(1), and 45(1) T at 4.2 K. Once again the relative areas of these sextets have been constrained to the iron occupancy of these sites as given above. Finally, because the

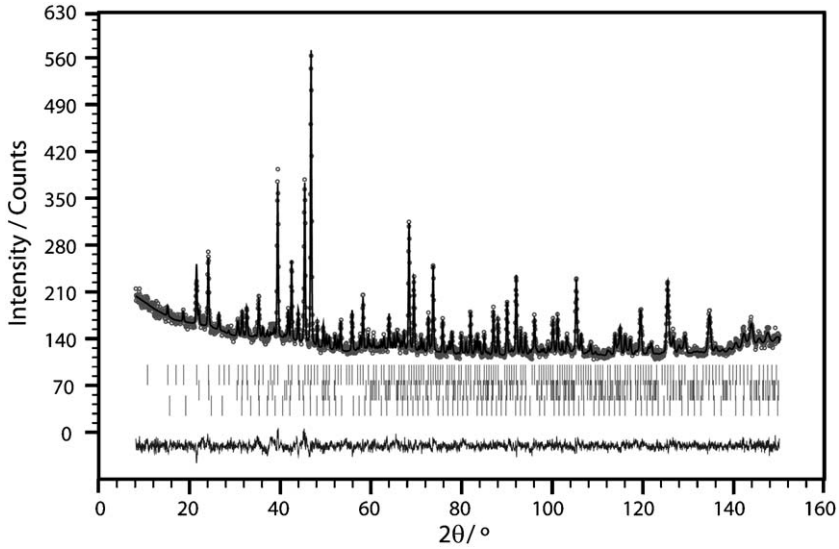

Fig. 2. Observed, calculated and difference neutron powder diffraction patterns of $Pr_{18}Li_8Fe_4RuO_{39}$ at room temperature. Vertical bars mark reflection positions for, in descending order; the principal phase, Li_2CO_3 and $LiFe_5O_8$.

Table 3
Unit-cell parameters and magnetic parameters of $Pr_{18}Li_8Fe_{5-x}M_xO_{39}$.

	M				
	Ru	Mn		Co	
	$x=1$	$x=1$	$x=2$	$x=1$	$x=2$
a/Å	12.0318(2)	11.9845(2)	11.9757(1)	11.96285(9)	11.94036(6)
C/cm^3 K mol^{-1}	42.00(8)	41.1(2)	39.2(2)	41.7(2)	38.84(8)
θ/K	−30.3(3)	−22.2(6)	−27.1(1)	−46.7(9)	−41.5(5)
T_f/K[a]	7.0(3)	5.0(3)	5.5(3)	5.5(3)	2.8(3)
κ	0.016	0.034	0.036	0.047	0.083

[a] Value determined from dc magnetometry data.

quadrupole shifts of the 2*a* and 16*i* sites are very poorly determined, for the fit of these two spectra, θ, the angle between any magnetic easy-axis and the principal axis of the electric field gradient at the iron, for the 2*a* and 16*i* sites, has been constrained to be the same as the 47.7° angle found for the 8*e* site. Rather unexpectedly, the 7 and 4.2 K spectra also revealed the presence of a paramagnetic component of 7% and 2% relative area, respectively, an area that has been included in the area of the 8*e* site in the fits shown in Fig. 7. The 7 and 4.2 K line widths, see Table 4, exhibit a significant broadening as compared with both the line widths observed above 25 K and the instrumental line width of 0.25(1) mm/s, a broadening that results from a small distribution in the hyperfine fields as a result of cation disorder.

The 12 K spectrum of $Pr_{18}Li_8Fe_4RuO_{39}$, see Fig. 7, is rather different from those observed at higher and lower temperatures. This spectrum shows the presence of a magnetic sextet, with a field of 48(1) T and a relative area of 39%, an area that has been assigned to the 8*e* site. The 2*a* and 16*i* spectral components, as well as the remaining 30% of the 8*e* spectral component, experience a small hyperfine field of 1.8 T, presumably a transferred field resulting from the 39% of the iron that exhibits a static hyperfine field at 12 K.

Both the isomer shifts and hyperfine fields observed for $Pr_{18}Li_8Fe_4RuO_{39}$ are compatible with the presence of iron(IV) on the 2*a* site and high-spin iron(III) on the 8*e* and 16*i* sites. In contrast to the spectral parameters obtained [2] for $Nd_{18}Li_8Fe_5O_{39}$, which indicated that the iron(IV) was low-spin, the 2*a* site parameters measured above 25 K for $Pr_{18}Li_8Fe_4RuO_{39}$ are consistent with the presence of either high-spin or low-spin iron(IV). However, the higher hyperfine field of 42(1) T observed at 4.2 K in $Pr_{18}Li_8Fe_4RuO_{39}$, as compared to the field of 20.3(3) T observed [2] in $Nd_{18}Li_8Fe_5O_{39}$, seems to support the presence of high-spin iron(IV) in $Pr_{18}Li_8Fe_4RuO_{39}$.

Confidence in the model used for the Mössbauer spectral fits described above may be obtained through the temperature dependence of the isomer shifts, δ, observed for the 2*a*, 8*e*, and 16*i* sites, and their weighted average values, see Fig. 8. As expected [2], the three isomer shifts are almost constant between 4.2 and 100 K but decrease slightly above 100 K as the result of the second-order Doppler shift. The temperature dependence of the isomer shift has been fit with the Debye model which yields Θ, a temperature that is characteristic of the lattice properties of the solid. The results of these fits are shown as the solid lines in Fig. 8 and yield, for the 2*a*, 8*e*, and 16*i* sites, and their weighted average isomer shifts, Θ values of 1100(200), 640(30), 730(100), and 710(40) K, respectively. These values are reasonable for oxides and similar within the error limits and vary in the same order as those observed [2] for $Nd_{18}Li_8Fe_5O_{39}$. The value for the 2*a* site is larger because it is associated with iron(IV) that is more tightly bound into the lattice than the iron(III) ions on the 8*e* and 16*i* sites.

(iii) $Pr_{18}Li_8Fe_{5-x}Mn_xO_{39}$ ($1 \leqslant x \leqslant 2$). X-ray diffraction analysis of reaction products in the $Pr_{18}Li_8Fe_{5-x}Mn_xO_{39}$ system indicated that monophasic, highly crystalline samples having the desired crystal structure had formed for $x=1$ and 2; the unit-cell parameter refined to the values listed in Table 3. A full structure refinement based on the X-ray data was not possible, partly because of the imbalance in the scattering lengths of lithium, oxygen and praseodymium and partly because of the lack of contrast between the scattering lengths of iron and manganese.

A maximum is observed (Fig. 10) in the ZFC susceptibility of both compositions at the temperature T_f listed in Table 3; the value of χ_{max} decreases as the concentration of manganese in the samples increases. The FC susceptibilities become essentially independent of temperature on cooling below T_f. On cooling the ZFC and FC susceptibilities are observed to diverge slightly above T_f, at ~7 K, although this is much more obvious in the case of the iron-rich composition $x=1$ for which the temperature width of the transition is significantly broader. In both cases the inverse susceptibility is a linear function of temperature above 100 K, and fitting to a Curie–Weiss law resulted in the parameters presented in Table 3. At a temperature of 2 K the magnetization of both

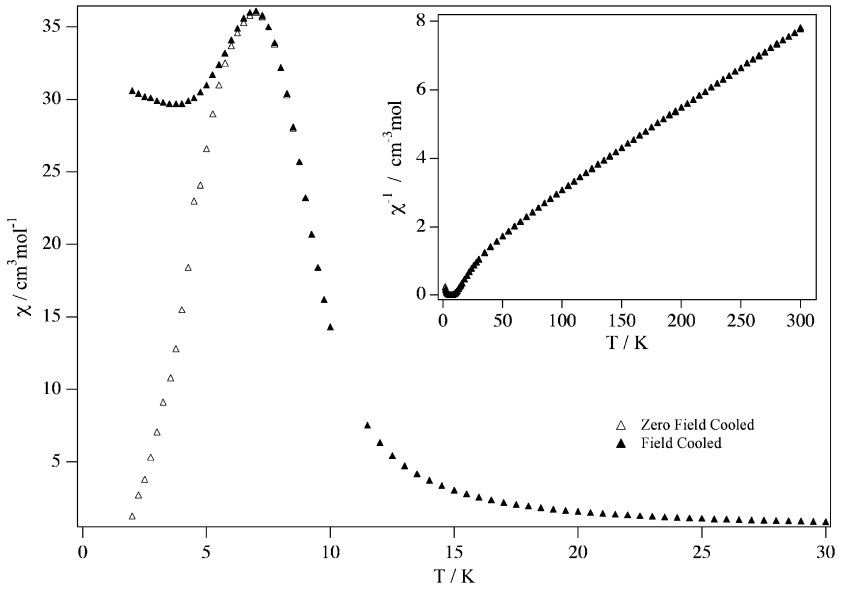

Fig. 3. Temperature dependence of the dc molar magnetic susceptibility of $Pr_{18}Li_8Fe_4RuO_{39}$; solid and hollow symbols represent FC and ZFC data, respectively. The inverse susceptibility is inset.

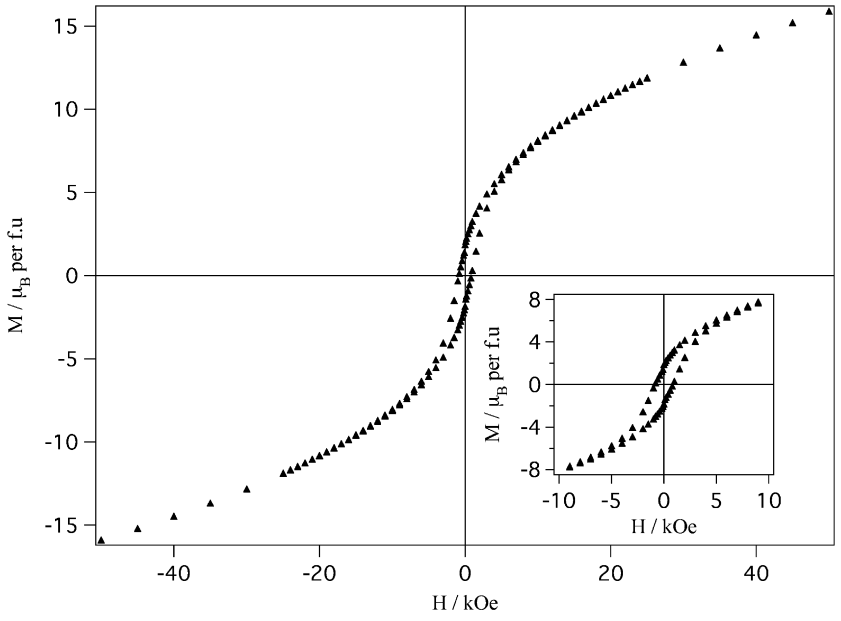

Fig. 4. Field dependence of the magnetization per formula unit of $Pr_{18}Li_8Fe_4RuO_{39}$ at 2 K.

samples is a non-linear function of field. At low fields both compositions show hysteresis in $M(H)$ and, as seen in Fig. 11, the effect is again more pronounced in the case of $Pr_{18}Li_8Fe_4MnO_{39}$.

The ac susceptibilities of both compositions in the $Pr_{18}Li_8Fe_{5-x}Mn_xO_{39}$ system show a similar dependence on temperature and frequency; this is illustrated in Fig. 12 for the composition $x = 1$. A maximum is observed in χ' at a frequency-dependent temperature close to T_f, and a maximum is also observed in χ''; the maximum in the real component of the ac susceptibility is co-incident with the minimum in the differential of the imaginary component for all frequencies in both compositions. The extent of the frequency dependence of T_f and hence the value of the parameter $\kappa = \Delta T_f/T_f\Delta \log \omega$ (Table 3) are essentially the same for both compositions. Above T_f χ'' falls to zero and no further frequency dependence is observed in either χ' or χ''. In contrast to $Pr_{18}Li_8Fe_4RuO_{39}$, both compositions show only one maximum in the imaginary susceptibility below T_f.

(iv) $Pr_{18}Li_8Fe_{5-x}Co_xO_{39}$ ($1 \leqslant x \leqslant 2$): X-ray diffraction analysis of reaction products in the $Pr_{18}Li_8Fe_{5-x}Co_xO_{39}$ system indicated that monophasic, highly crystalline samples having the desired crystal structure had formed for $x = 1$ and 2; the unit-cell parameter refined to the values listed in Table 3. As in the case of $Pr_{18}Li_8Fe_{5-x}Mn_xO_3$ a full structure refinement based on the X-ray data was not possible. A $LiCoO_2$ impurity phase was detectable in compositions having $x > 2$. The temperature dependence of the dc susceptibilities of $Pr_{18}Li_8Fe_4CoO_{39}$ and $Pr_{18}Li_8Fe_3Co_2O_{39}$ is shown in Fig. 13. In both cases the ZFC and the FC susceptibilities differ below 12 K. The former shows a maximum at T_f (Table 3) whereas the latter continues to increase down to the lowest temperature measured. The data

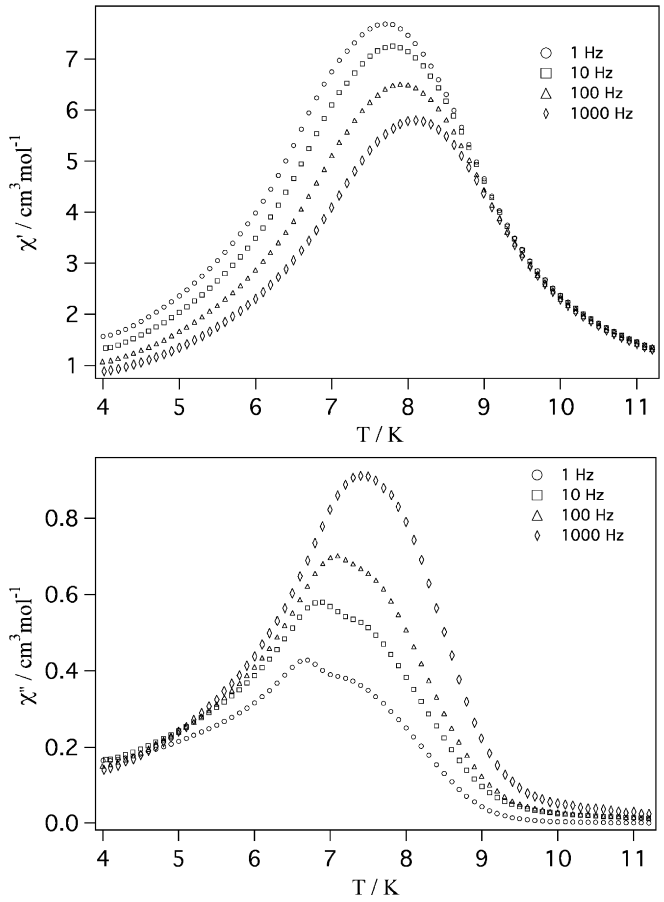

Fig. 5. Temperature and frequency dependence of the real (upper) and imaginary (lower) components of the ac molar susceptibility of $Pr_{18}Li_8Fe_4RuO_{39}$.

collected on both samples in the temperature region $100 < T/K < 300$ were fitted to a Curie–Weiss law; the resulting parameters are included in Table 3. At a temperature of 2 K the magnetization of both samples is a non-linear function of field. At low fields both compositions show hysteresis in $M(H)$; the effect is more pronounced (Fig. 14) in the case of $Pr_{18}Li_8Fe_4CoO_{39}$. Neither composition shows magnetic saturation in a field of 50 kOe.

In view of the similar behaviour of the two compositions, ac susceptibility data are only shown for the composition $x = 1$ (Fig. 15); the derived parameters for both compositions are listed in Table 3. A maximum is observed in χ' at a frequency-dependent temperature T_f, and a maximum is also observed in χ''; the maximum in the real component of the ac susceptibility is coincident with the minimum in the differential of the imaginary component for all frequencies in both compositions. The value of the parameter $\kappa = \Delta T_f / T_f \Delta \log \omega$ that quantifies the frequency dependence of T_f is given in Table 3. Above T_f χ'' falls to zero and no further frequency dependence is observed in either χ' or χ''.

4. Discussion

Our failure to date to prepare a monophasic sample of $Pr_{18}Li_8Fe_5O_{39}$ contrasts with the successful synthesis of $Nd_{18}Li_8Fe_5O_{39}$ and thus demonstrates that, as suggested above, the stability of these systems is very sensitive to the properties of the lanthanide element present. Further evidence of this sensitivity is provided by our study of the ruthenium-containing compositions. We have now prepared $Pr_{18}Li_8Fe_4RuO_{39}$ although we have not been able to prepare $Nd_{18}Li_8Fe_4RuO_{39}$ by the same method. The limited composition range found for the $Pr_{18}Li_8Fe_{5-x}Ru_xO_{39}$ system can be attributed to the redox chemistry of the two transition elements and, in particular, to the difficulty in stabilizing Ru^{3+} in mixed-metal oxides [9–13].

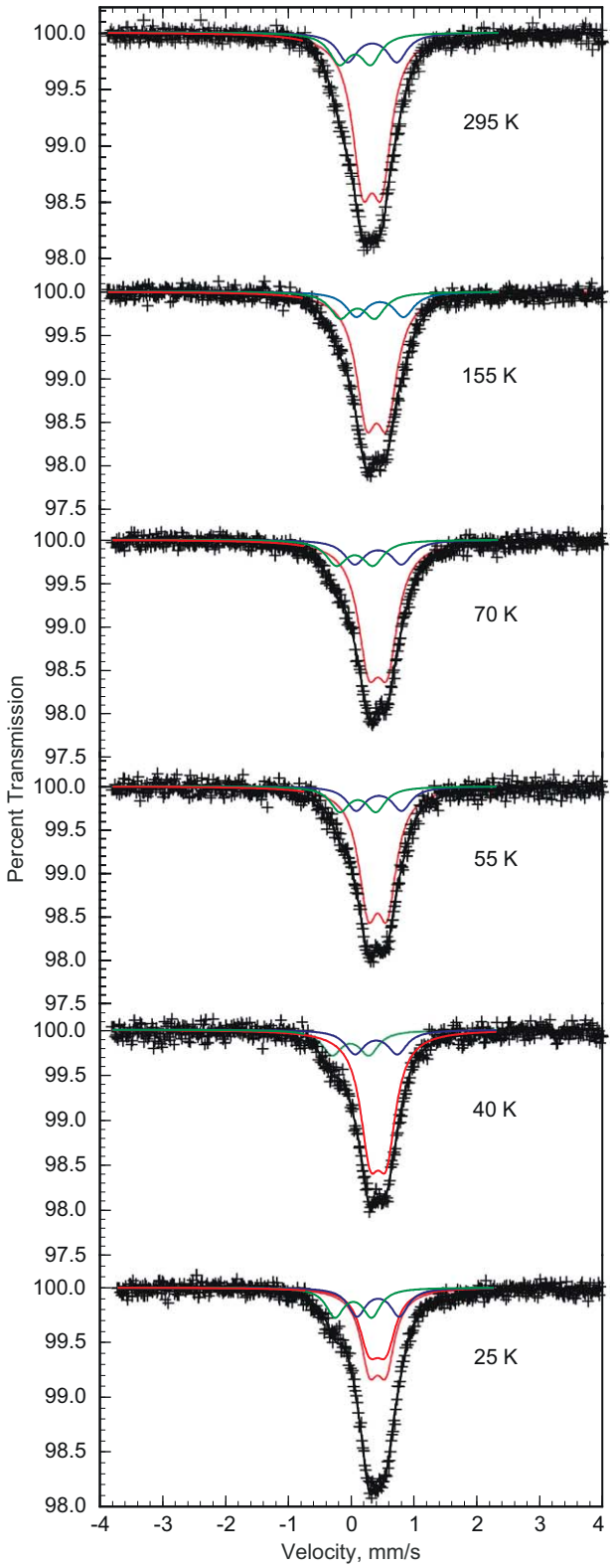

Fig. 6. The iron-57 Mössbauer spectra of $Pr_{18}Li_8Fe_4RuO_{39}$ measured at the indicated temperatures. The green, red, and blue lines correspond to the components assigned to the 2*a*, 8*e*, and 16*i* sites, respectively.

The refined crystal structure of $Pr_{18}Li_8Fe_4RuO_{39}$ is very similar in many ways to other members of this structural family that have been described elsewhere [1–3], although the unit-cell parameter (Table 3) is perhaps unexpectedly large. It is not surprising, given the presence of a second-row transition metal, that the value is larger than those of the other compounds described in this work but the increase is sufficient for the unit-cell parameter of $Pr_{18}Li_8Fe_4RuO_{39}$ to match that of $Pr_{18}Li_8Rh_4MnO_{39}$ ($a = 12.0317(1)$ [14]). The lithium-iron site exchange between the 8*e* and 16*i* sites is a common feature of these structures and tends to occur whenever the 8*e* site is large enough to accommodate the Li^+ cation. The mean metal-to-oxygen bond length around this site (2.042 Å) in $Pr_{18}Li_8Fe_4RuO_{39}$ is consistent with this observation. The mean bond lengths around the ions Pr1 and Pr2 are consistent with those reported previously [15], although the Pr2–O4 distance is relatively short. Interestingly, this strong interaction between the *Ln*–O framework and an anion that forms part of the polyhedral chains has not been observed in the neodymium compounds studied to date. The Pr–O bond lengths are all longer than those observed (~2.22 Å) in the Pr(IV) compound $BaPrO_3$ [16]. Perhaps the most surprising aspect of the structural chemistry of $Pr_{18}Li_8Fe_4RuO_{39}$ is the presence of Fe^{4+} on the 2*a* site when our knowledge of the oxide chemistry of iron and ruthenium led us to anticipate that any successful synthesis

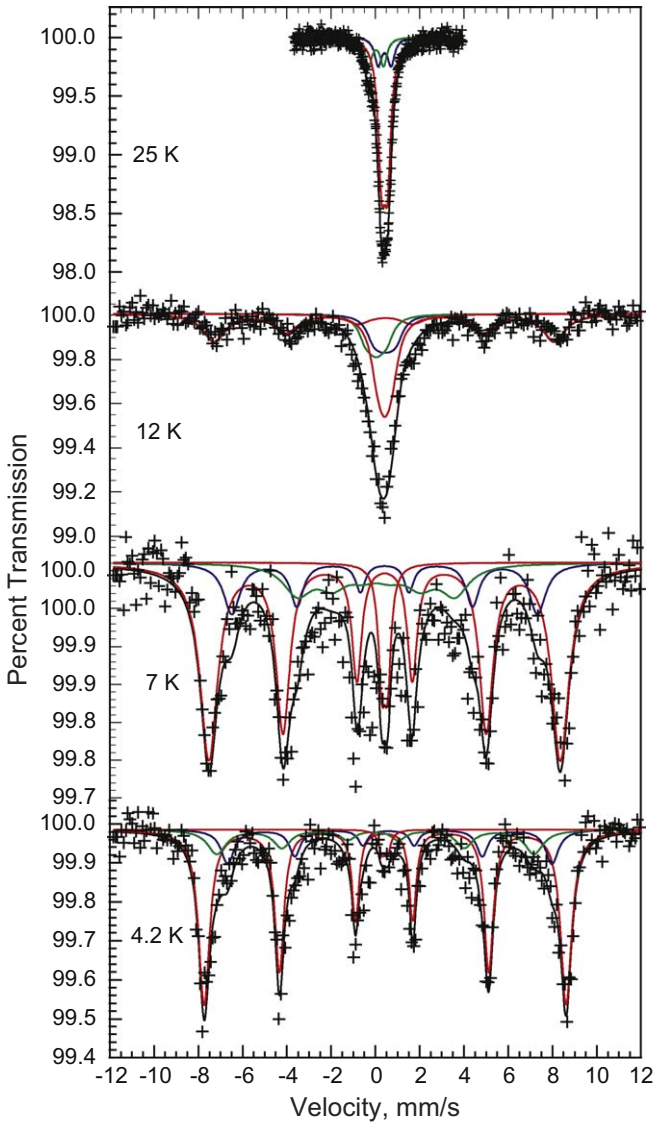

Fig. 7. The iron-57 Mössbauer spectra of $Pr_{18}Li_8Fe_4RuO_{39}$ measured at the indicated temperatures. The green, red, and blue lines correspond to the components assigned to the 2*a*, 8*e*, and 16*i* sites, respectively.

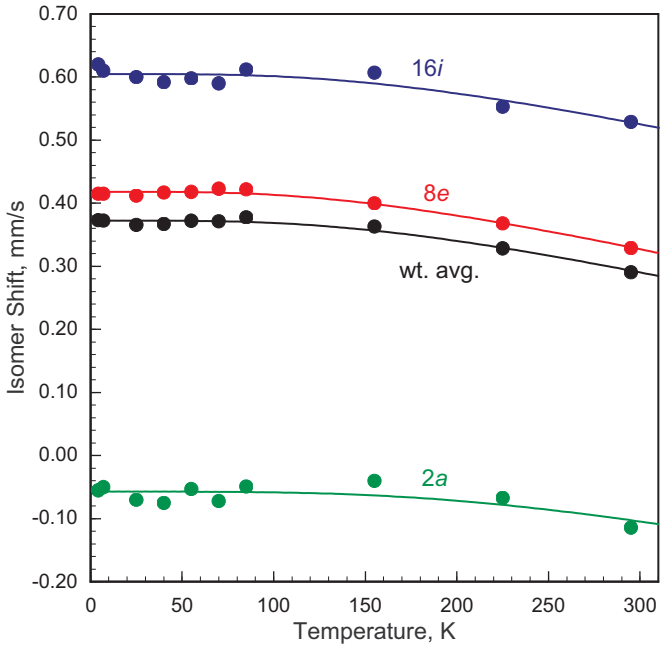

Fig. 8. The temperature dependence of the Mössbauer spectral isomer shifts for the 2*a*, 8*e*, and 16*i* sites, and their weighted average, in $Pr_{18}Li_8Fe_4RuO_{39}$. The solid lines correspond to fits with the Debye model for a solid and the absolute errors are approximately twice the size of the data points.

Table 4
Mössbauer spectral parameters for $Pr_{18}Li_8Fe_4RuO_{39}$.

T (K)	2*a* site			8*e* site			16*i* site		
	δ (mm/s[a])	ΔE_Q (mm/s)	Γ (mm/s)	δ (mm/s)[a]	ΔE_Q (mm/s)	Γ (mm/s)	δ (mm/s)[a]	ΔE_Q (mm/s)	Γ (mm/s)
295	−0.114	0.140	0.39	0.329	0.300	0.39	0.53	0.41	0.39
225	−0.067	0.191	0.41	0.368	0.313	0.41	0.55	0.42	0.41
155	−0.040	0.245	0.40	0.400	0.321	0.40	0.61	0.46	0.40
85	−0.049	0.248	0.40	0.422	0.324	0.40	0.61	0.45	0.40
70	−0.072	0.284	0.40	0.423	0.300	0.40	0.59	0.46	0.40
55	−0.053	0.279	0.38	0.418	0.296	0.38	0.60	0.41	0.38
40	−0.075	0.326	0.35	0.417	0.287	0.35	0.59	0.36	0.35
25	−0.070	0.433	0.38	0.412	0.262	0.38	0.60	0.34	0.38
7	−0.050	0.585	1.54	0.415	0.262	0.39	0.61	0.32	0.46
4.2	−0.055	0.585	0.78	0.415	0.262	0.44	0.62	0.32	0.47

[a] The isomer shifts are given relative to room temperature α-iron powder.

would result in a compound containing only Fe^{3+} and Ru^{4+} in a 4:1 ratio. Furthermore, the Mössbauer spectra show that the Fe^{4+} cations are in a high-spin state, whereas they occur in a low-spin state in analogous compounds that have been studied previously. The observation of a metal–oxygen bond length around the 2*a* site (1.90(1) Å) that is longer than those observed previously is consistent with this conclusion. This expansion of the Fe(Ru)–O4 bond length is perhaps largely responsible for the marked increase in the unit-cell parameter noted above. The observed Fe(Ru)–O4 bond length is slightly shorter than the Fe–O bond measured [17] in $CaFeO_3$ (1.92 Å), and it is significantly shorter than the Ru–O distances measured in $BaRuO_3$ [18,19] and $SrRuO_3$ [20]. This suggests that, as in the compounds studied previously, the 2*a* site is subjected to considerable chemical pressure although in the present case it is insufficient to drive a spin-state transition in Fe^{4+}. The Pr–Pr distance across the diameter of one of the channels gives a measure of this pressure; the distance of 6.321 Å observed in this compound is significantly larger than those observed in the Nd-containing analogues, for example 6.282 Å in $Nd_{18}Li_8Fe_5O_{39}$. A corollary of the presence of Fe^{4+} is that Ru^{3+} must be present on the 8*e* site in order to maintain charge neutrality. This cation is not usually found in oxides prepared in air [9–13], and further spectroscopic studies are necessary in order to prove beyond doubt that it is present in this compound. An alternative explanation is that the compound is iron deficient, thus allowing all the ruthenium to exist as Ru^{4+}. The presence of the $LiFe_5O_8$ impurity is qualitatively consistent with this explanation, but the observed impurity level is significantly lower than that required for complete oxidation to Ru^{4+}. The inverse analysis, in which the observed impurity level is used to calculate the iron deficiency, results in a concentration of Fe^{4+} that is inconsistent with the Mössbauer spectra. Thus, although our sample might be iron-deficient, the level of the deficiency is too small to eliminate completely the need to invoke the presence of Ru^{3+}.

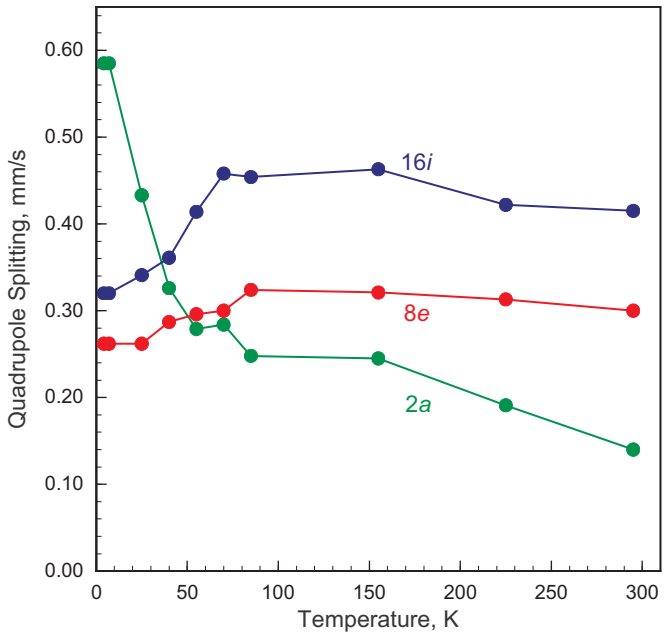

Fig. 9. The temperature dependence of the Mössbauer spectral quadrupole splittings for the 2*a*, 8*e*, and 16*i* sites in $Pr_{18}Li_8Fe_4RuO_{39}$. The error bars are approximately twice the size of the data points.

The negative Weiss temperature ($\theta = -30.3$ K) of $Pr_{18}Li_8Fe_4RuO_{39}$ demonstrates that antiferromagnetic interactions are dominant in this compound. The molar Curie constant (42.0 $cm^3\,K\,mol^{-1}$) is reduced below the value (45.1 $cm^3\,K\,mol^{-1}$) calculated assuming the presence of high-spin iron and low-spin ruthenium cations. Similar reductions observed in related compounds have been ascribed to high-temperature, short-range antiferromagnetic coupling between Fe^{3+} cations separated by only ~2.44 Å in face-sharing polyhedra; the short Fe^{3+}–Fe^{3+} contact arises as a consequence of iron–lithium site exchange. The presence of a magnetic cation on a prismatic site frustrates the envisaged pattern of simple antiferromagnetic coupling between nearest-neighbour, octahedrally-coordinated transition-metal cations and there is no evidence to suggest that the desired ferrimagnetic ordering occurs in this compound at low temperatures. The frequency dependence of T_f (Fig. 5), parameterized by κ (Table 3), is indicative of the formation of a spin-glass-like state, as are the irreversible but unsaturated form of the function $M(H)$ and the inequivalence of the ZFC and FC dc susceptibilities below T_f. The origin of the fine structure in χ'' is not clear, but it might

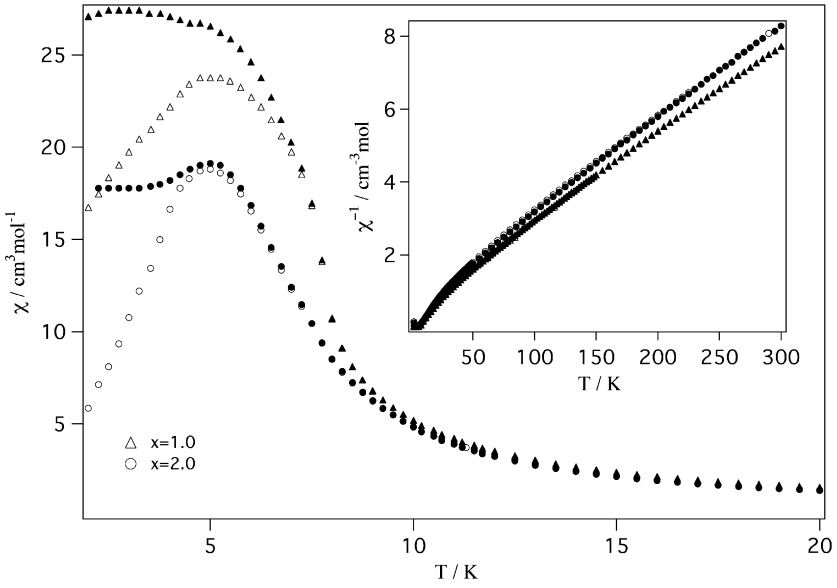

Fig. 10. Temperature dependence of the dc molar magnetic susceptibility of $Pr_{18}Li_8Fe_{5-x}Mn_xO_{39}$; solid and hollow symbols represent FC and ZFC data, respectively. The inverse susceptibilities are inset.

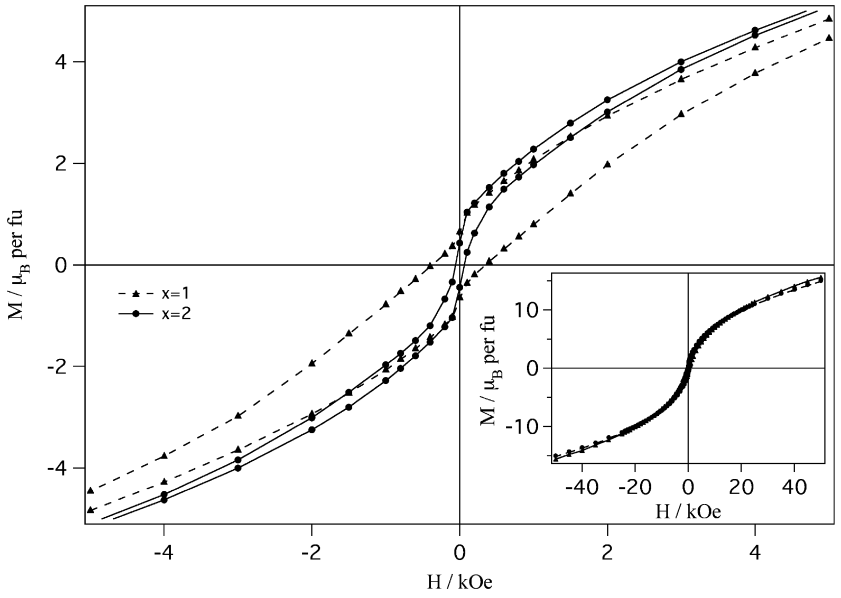

Fig. 11. Field dependence of the magnetization per formula unit of $Pr_{18}Li_8Fe_{5-x}Mn_xO_{39}$ at 2 K.

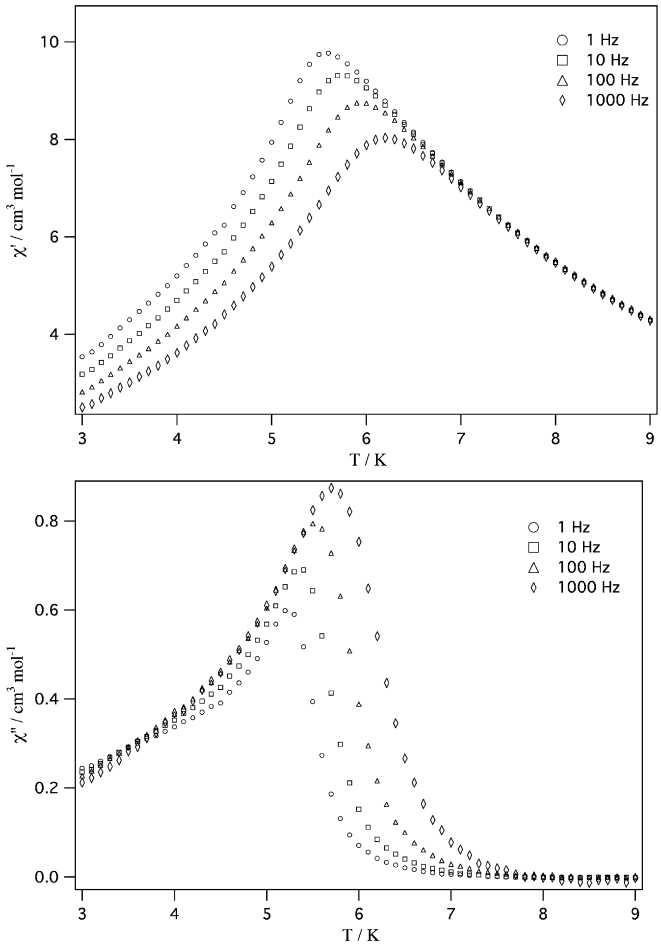

Fig. 12. Temperature and frequency dependence of the real (upper) and imaginary (lower) components of the ac molar susceptibility of $Pr_{18}Li_8Fe_4MnO_{39}$.

signify that the atomic moments on the different sublattices show different relaxation properties. The overall decrease in the magnetic susceptibility on cooling below T_f shows that the atomic moments of the Fe^{3+}, Ru^{4+} and Pr^{3+} cations all take part in the freezing process but the Mössbauer spectrum collected at 12 K provides clear evidence that slow spin relaxation persists to higher temperatures for the iron located on the 8*e* sites. However, some of these spins remain paramagnetic down to 4.2 K, suggesting that the structural disorder creates a range of local environments around the 8*e* sites, including some that experience only very weak superexchange interactions. Alternatively, a range of particle sizes in the sample might lead to a range of transition temperatures, with 2.25% of the iron remaining paramagnetic to 4.2 K. It is not clear whether the unusual temperature dependence of χ'' below T_f is another symptom of this behaviour. The magnetometry data collected on $Pr_{18}Li_8Fe_4RuO_{39}$ are very similar to those collected on related systems, for example $Nd_{18}Li_8Fe_5O_{39}$ and $Nd_{18}Li_8Fe_4MnO_{39}$. In these cases the absence of long-range magnetic order and the presence of slow spin relaxation were confirmed by neutron diffraction and Mössbauer spectroscopy, respectively. In all these cases our aim was to make a ferrimagnet by ordering two different transition-metal cations over the 2*a* and 8*e* sites. The formation once again of a spin-glass-like phase by $Pr_{18}Li_8Fe_4RuO_{39}$ is most likely to be attributable to the magnetic frustration introduced by the cation disorder. We have used a similar argument before to explain the behaviour of $Nd_{18}Li_8Fe_5O_{39}$. In that compound the 2*a* site is occupied by Fe^{4+} and the majority of the 8*e* sites are occupied by Fe^{3+}. However, lithium–iron site exchange occurs and glassy behaviour results. The behaviour of the dc susceptibility of $Pr_{18}Li_8Fe_4RuO_{39}$ also resembles that reported previously for a series of $A_3BB'O_6$ compounds in which transition-metal cations (B, B′) occupy, in a disordered manner, both the octahedral and the prismatic sites in similar polyhedral chains [21,22]. We note also that our original strategy assumed that only the magnetic coupling between cations in linear ⟨111⟩ chain segments needed to be considered. Magnetic coupling involving the lanthanide cations and the possibility of superexchange coupling between cations located on intersecting diagonals of the cube were both ignored: if either has a significant strength it would constitute another source of frustration.

Whereas $Nd_{18}Li_8Fe_{5-x}Mn_xO_{39}$ and $Nd_{18}Li_8Fe_{5-x}Co_xO_{39}$ could be synthesized [3] for $x \leqslant 4$, the compositions $Pr_{18}Li_8Fe_{5-x}Mn_xO_{39}$ and $Pr_{18}Li_8Fe_{5-x}Co_xO_{39}$ could be prepared only for $x \leqslant 2$. This, together with our failure to prepare $Nd_{18}Li_8Fe_4RuO_{39}$, emphasizes

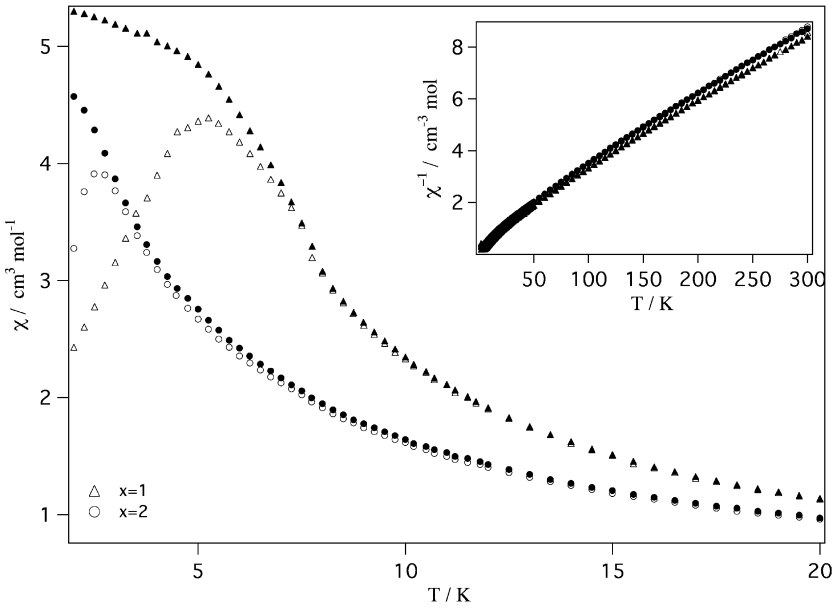

Fig. 13. Temperature dependence of the dc molar magnetic susceptibility of $Pr_{18}Li_8Fe_{5-x}Co_xO_{39}$; solid and hollow symbols represent FC and ZFC data, respectively. The inverse susceptibilities are inset.

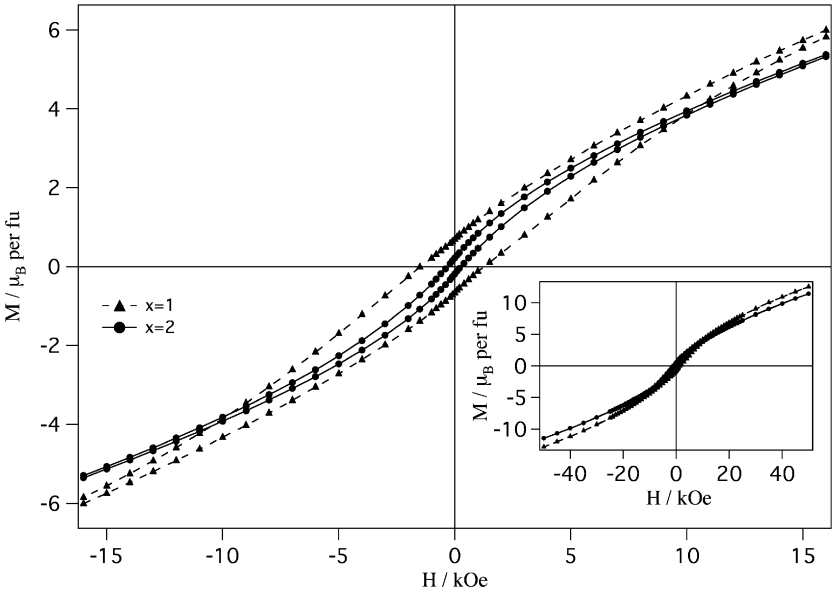

Fig. 14. Field dependence of the magnetization per formula unit of $Pr_{18}Li_8Fe_{5-x}Co_xO_{39}$ at 2 K.

the need to match the size of the lanthanide element to the size of the transition metals when synthesizing these phases. However, the magnetic behaviour of the praseodymium compositions is very similar to that shown by the neodymium analogues. The evidence presented in Figs. 11–15 and Table 3 shows that these are spin-glass-like materials with freezing temperatures below 6 K. In the absence of the sought-after ferrimagnetism, no attempt was made to characterize these compositions further by neutron diffraction or Mössbauer spectroscopy. However, we note that, as in the case of the neodymium analogues, the unit-cell parameter decreases as iron is progressively substituted by either manganese or cobalt, despite the fact that any cation of manganese would be expected to be larger than the analogous iron species. This might be a consequence of changes in the Fe:M ratio on the 2*a* site, and also of changes in the degree of lithium–iron site exchange. The more extensive data [3] available for the $Nd_{18}Li_8Fe_{5-x}Mn_xO_{39}$ system showed that site exchange does not occur in $Nd_{18}Li_8FeMn_4O_{39}$ and we were able to show that our data were consistent with the presence of low-spin Mn^{3+}. This would be consistent with the composition dependence of the lattice parameter of $Pr_{18}Li_8Fe_{5-x}Mn_xO_{39}$, but we do not have sufficient data to make the same argument in the present case.

To summarize, this study has demonstrated that the size of the lanthanide cation is important in determining whether a particular composition in the $Ln_{18}Li_8M_4M'O_{39}$ family can be synthesized, and that consideration must be given to the relative sizes of *Ln*, M and M′. However, the magnetic properties of these compositions, once formed, show very little dependence on the lanthanide element, although the latter is clearly involved in the spin-freezing process that has been observed at low temperatures.

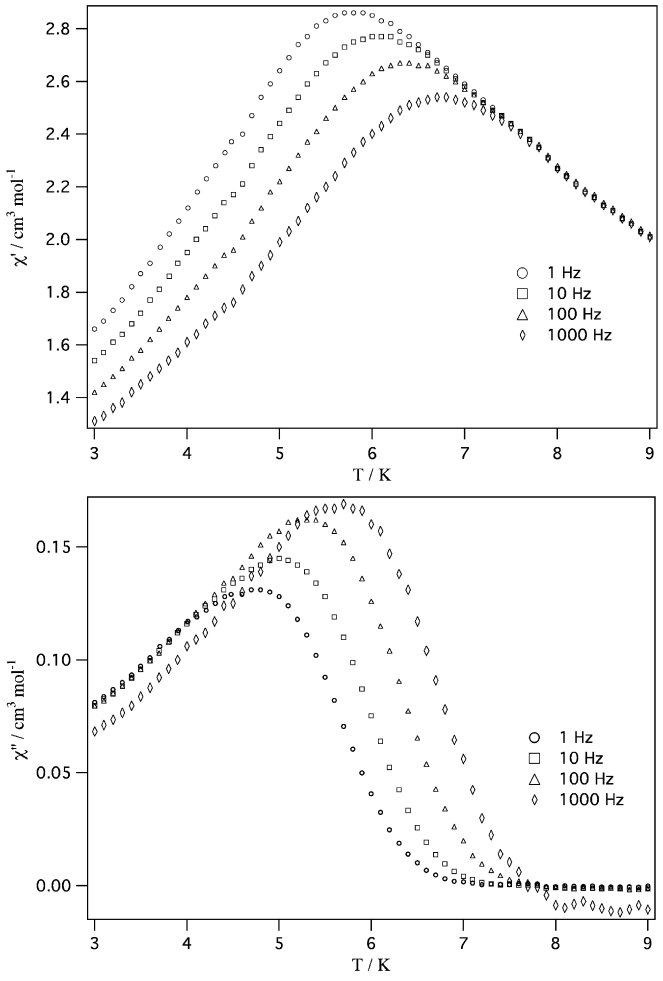

Fig. 15. Temperature and frequency dependence of the real (upper) and imaginary (lower) components of the ac molar susceptibility of $Pr_{18}Li_8Fe_4CoO_{39}$.

Acknowledgments

We are grateful to Somerville College, Oxford and EPSRC for the provision of a studentship for SED. We acknowledge the experimental assistance provided by Clemens Ritter at ILL, Grenoble. F.G. thanks the Fonds National de la Recherche Scientifique of Belgium (Grants 9.456595 and 1.5.064.05) for financial support.

References

[1] P.P.C. Frampton, P.D. Battle, C. Ritter, Inorganic Chemistry 44 (2005) 7138.
[2] S.E. Dutton, P.D. Battle, F. Grandjean, G.J. Long, K. Oh-ishi, Inorganic Chemistry 47 (2008) 11212.
[3] S.E. Dutton, P.D. Battle, F. Grandjean, G.J. Long, P.A. van Daesdonk, Inorganic Chemistry 48 (2009) 1613.
[4] J.A. Rodgers, P.D. Battle, N. Dupre, C.P. Grey, J. Sloan, Chemistry of Materials 16 (2004) 4257.
[5] H.M. Rietveld, Journal of Applied Crystallography 2 (1969) 65.
[6] A.C. Larson, R.B. von-Dreele, General structure analysis system (GSAS), Report LAUR 86-748, Los Alamos National Laboratories, 1994.
[7] J. Rodriguez-Carvajal, Physica B 192 (1993) 55.
[8] A. Tomas, P. Laruelle, J.L. Dormann, M. Nogues, Acta Crystallographica Section C 39 (1983) 1615.
[9] R.J. Bouchard, J.F. Weiher, Journal of Solid State Chemistry 4 (1972) 80.
[10] F.M. da Costa, R. Greatrex, N.N. Greenwood, Journal of Solid State Chemistry 20 (1977) 381.
[11] R. Greatrex, G. Hu, D.C. Munro, Materials Research Bulletin 21 (1986) 797.
[12] N.N. Greenwood, F.D. de A. da Costa, R. Greatrex, Revue De Chimie Minérale 13 (1976) 133.
[13] H. Kobayashi, M. Nagata, R. Kanno, Y. Kawamoto, Materials Research Bulletin 29 (1994) 1271.
[14] S.E. Dutton, D.Phil. Thesis, University of Oxford, 2009.
[15] M. Marezio, J.P. Remeika, P.D. Dernier, Acta Crystallographica Section B 26 (1970) 2008.
[16] A.J. Jacobson, B.C. Tofield, B.E.F. Fender, Acta Crystallographica Section B 28 (1972) 956.
[17] T. Takeda, R. Kanno, Y. Kawamoto, M. Takano, S. Kawasaki, T. Kamiyama, F. Izumi, Solid State Sciences 2 (2000) 673.
[18] S. Hong, A.W. Sleight, Journal of Solid State Chemistry 128 (1997) 251.
[19] N. Tancret, P. Roussel, F. Abraham, Journal of Solid State Chemistry 177 (2004) 808.
[20] C.W. Jones, P.D. Battle, P. Lightfoot, W.T.A. Harrison, Acta Crystallographica Section C 45 (1989) 365.
[21] H. Kageyama, K. Yoshimura, K. Kosuge, Journal of Solid State Chemistry 140 (1998) 14.
[22] S. Niitaka, H. Kageyama, M. Kato, K. Yoshimura, K. Kosuge, Journal of Solid State Chemistry 146 (1999) 137.